Supplemental Material: Exploring the Equivalence between Two-dimensional Classical and Quantum Turbulence through Velocity Circulation Statistics

Nicolás P. Müller[1, 2] and Giorgio Krstulovic[1]

[1] *Université Côte d'Azur, Observatoire de la Côte d'Azur, CNRS, Laboratoire Lagrange, Boulevard de l'Observatoire CS 34229 - F 06304 NICE Cedex 4, France*

[2] *Laboratoire de Physique de l'École normale supérieure, ENS, Université PSL, CNRS, Sorbonne Université, Université de Paris, Paris, France*

(Dated: December 12, 2023)

GENERATION OF 2D INITIAL CONDITION

We study the statistical properties of two-dimensional (2D) quantum turbulence (QT) by performing direct numerical simulations of the Gross–Pitaevksii (GP) equation

$$i\partial_t\psi = \frac{c}{\sqrt{2}\xi}\left(-\xi^2\nabla^2\psi + \frac{|\psi|^2}{n_0}\psi - \psi\right) \tag{1}$$

with ψ the condensate wave function, c the speed of sound, ξ the healing length and n_0 the ground state particles density. We set $n_0 = 1$ and the healing length so that $\xi k_{\max} > 2$ to solve well the density profile of quantum vortices.

The total energy in the GP equation is conserved, with the incompressible energy being irreversibly transferred into sound. Therefore, when it comes to studying the quantum vortex dynamics, GP simulations can be seen as decaying quantum turbulent runs. Statistical properties of the flow are typically studied during a transient period in which turbulence is strongest. The implementation of an external forcing would also excite phonons that accelerate the process of vortex annihilation and contaminate the dynamics of quantum vortices.

To generate the 2D initial condition with the initial energy concentrated between some target wave numbers, we build a velocity field in the Clebsch representation $\boldsymbol{v} = \lambda\boldsymbol{\nabla}\mu - \boldsymbol{\nabla}\chi$ [1, 2], where the Clebsch potential are a linear combination of modes

$$\lambda = \frac{1}{2k_\lambda}\sum_{k_i=1}^{2k_\lambda}\cos\left\{x\left[k_\lambda\cos\left(\frac{\pi k_i}{2k_\lambda}\right)\right] + y\left[k_\lambda\sin\left(\frac{\pi k_i}{2k_\lambda}\right)\right] + \phi_{k_i}\right\} \tag{2}$$

$$\mu = \frac{1}{2k_\mu}\sum_{k_i=1}^{2k_\mu}\cos\left\{x\left[k_\mu\cos\left(\frac{\pi k_i}{2k_\mu}\right)\right] + y\left[k_\mu\sin\left(\frac{\pi k_i}{2k_\mu}\right)\right] + \varphi_{k_i}\right\} \tag{3}$$

where k_λ and k_μ set the maximum number of the superposition of modes for each Clebsch potential, ϕ_{k_i} and φ_{k_i} are random phase, and the square brackets [.] indicate the integer part of the argument to satisfy periodicity. The third Clebsch potential χ is defined so that the initial velocity field is incompressible $\boldsymbol{\nabla}\cdot\boldsymbol{v} = 0$. Different values of k_λ and k_μ will lead to different initial conditions with energy concentrated at different scales. The vorticity field is defined as $\boldsymbol{\omega} = \boldsymbol{\nabla}\times\boldsymbol{v} = \boldsymbol{\nabla}\lambda\times\boldsymbol{\nabla}\mu$. With these potentials, we can also construct a wave function ψ such that $\psi(x, y) = \psi_e(\lambda(x, y), \mu(x, y))$ where the ψ_e has zeros at the zeros of the Clebsch potentials, corresponding to quantum vortices with a non-zero vorticity field. The wave function is then constructed as $\psi_e(\lambda, \mu) = (\lambda + i\mu)\tanh\left[\sqrt{\lambda^2+\mu^2}/(\sqrt{2}\xi)\right]/\sqrt{\lambda^2+\mu^2}$. The choice of a hyperbolic tangent is done to give a good approximation of the quantum vortex density profiles. In practice, we can increase the number of vortices by multiplying several of these wave functions, for example, $\psi(x, y) = \Pi_{i=-1}^{1}\psi_e(\lambda - i, \mu - i)$.

As a final step, we want the wave function to follow the velocity field generated by the Clebsch potentials, with a minimal amount of acoustic emission. In particular, we generate initial flows with a Mach number $M = U/c \leq 0.3$ to neglect compressible effects. For this purpose, we first evolve the wave function using the advective real Ginzburg-Landau (ARGL) equation

$$\partial_t\psi = -\frac{c}{\sqrt{2}\xi}\left(-\xi^2\nabla^2\psi + \frac{|\psi|^2}{n_0}\psi - \psi\right) - i\boldsymbol{v}\cdot\boldsymbol{\nabla}\psi - \frac{(\boldsymbol{v})^2}{2\sqrt{2}c\xi}\psi. \tag{4}$$

Once the evolution of the ARGL equation is well converged, we evolve the system using the GP Eq. (1).

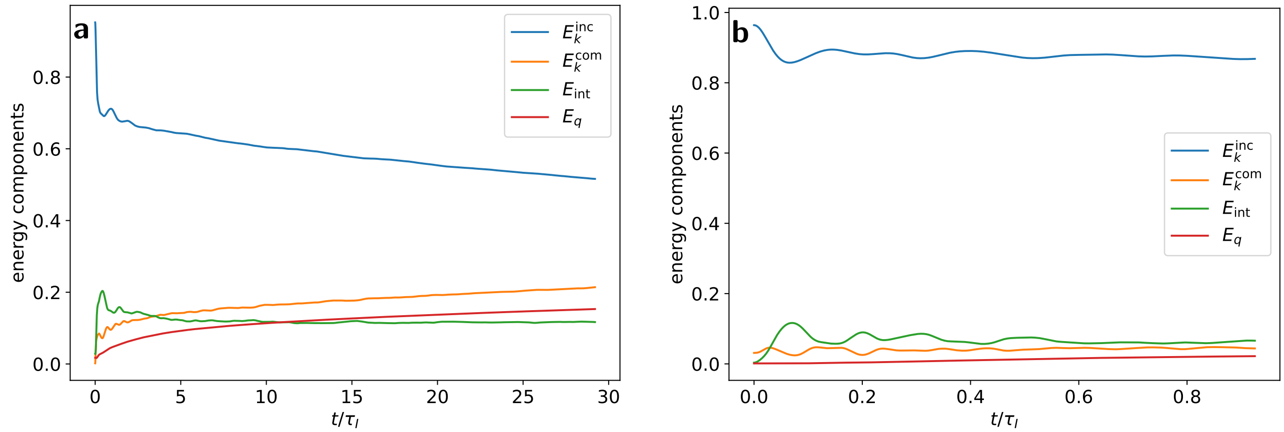

FIG. 1. Evolution of the incompressible, compressible, internal and quantum energy components in (a) the inverse energy cascade and (b) in the direct enstrophy cascade simulations with Mach number $M = 0.3$.

PARAMETERS OF THE NUMERICAL SIMULATIONS

To study the properties of 2D classical and quantum turbulence, we solve the GP equation incompressible Navier–Stokes (NS) equation, which in terms of the vorticity ω is written as

$$\partial_t \omega + \{\omega, \phi\} = \nu \nabla^2 \omega - \alpha \omega + f \tag{5}$$

with ϕ the stream function such that the velocity field is $(u, v) = (\partial_y \phi, -\partial_x \phi)$, the Poisson brackets are defined as $\{\omega, \phi\} = \partial_x \omega \partial_y \phi - \partial_y \omega \partial_x \phi$, ν is the kinematic viscosity, α is a linear friction preventing the formation of a large-scale condensate, and f an external forcing. We solve these equations using a standard pseudospectral method in a bi-periodic domain and a Runge–Kutta method for time stepping of order 2 for NS and order 4 for GP. We perform a total of four numerical simulations, two to study the inverse energy cascade (IEC), and another two for the direct enstrophy cascade (DEC). Out of these two, in one we solve the NS equation and in the other the GP equation.

For the NS IEC simulation, we force at small scales using a Gaussian forcing centered at $k_f = 637$ of width $\Delta k = 425$ with $N = 6144$ linear collocation points, $\nu = 8 \times 10^{-6}$ and $\alpha = 3.28 \times 10^{-2}$, while for the DEC we use a random forcing at $k_f = 1$ and $k_f = 2$ with $N = 6144$, $\nu = 5 \times 10^{-7}$ and $\alpha = 0$. Both of these regimes are studied in a stationary state and we use several hundred velocity fields to increase the amount of statistics. For the GP simulations, we use $N = 8192$ linear collocation points and set the healing length $\xi = 1.5\Delta x$, $n_0 = 1$ and the speed of sound $c = 1$, with $\Delta x = L/N$ and $L = 2\pi$ the size of the domain. To study the IEC, we generate an initial condition as described in the previous section, with wave numbers in a band around $k_{\mathrm{IC}} = 30$, and an initial Mach number $M = v_{\mathrm{rms}}/c = 0.3$. For the DEC we initialize a flow with wave numbers between $k_{\mathrm{IC}} = 1$ and $k_{\mathrm{IC}} = 2$, and $M = 0.29$. As these simulations are not in a stationary state, we only study small time intervals in which turbulence is stronger. To increase the amount of statistics, we perform an ensemble of four and five numerical simulations for the inverse and direct cascades, respectively. These runs are performed using different random phases for the initial conditions and are statistically equivalent. To study compressible effects, we compare some of the results with an ensemble of seven runs with initial Mach $M = 0.5$.

ENERGY AND ENSTROPHY EVOLUTION IN GROSS–PITAEVSKII

As the simulations of the GP equation are performed without any external forcing, there are different regimes that can be found in a 2D quantum turbulent flow [3]. Among these, there is first a regime in which the initial conditions of the system dominate, a turbulent regime, a decaying one and eventually for long times the system can thermalize due to finite size effects. In our case, we will study the statistical properties of the flow within a time window in which turbulence is strongest and when the system displays good Kolmogorov-like scaling properties. This is a standard

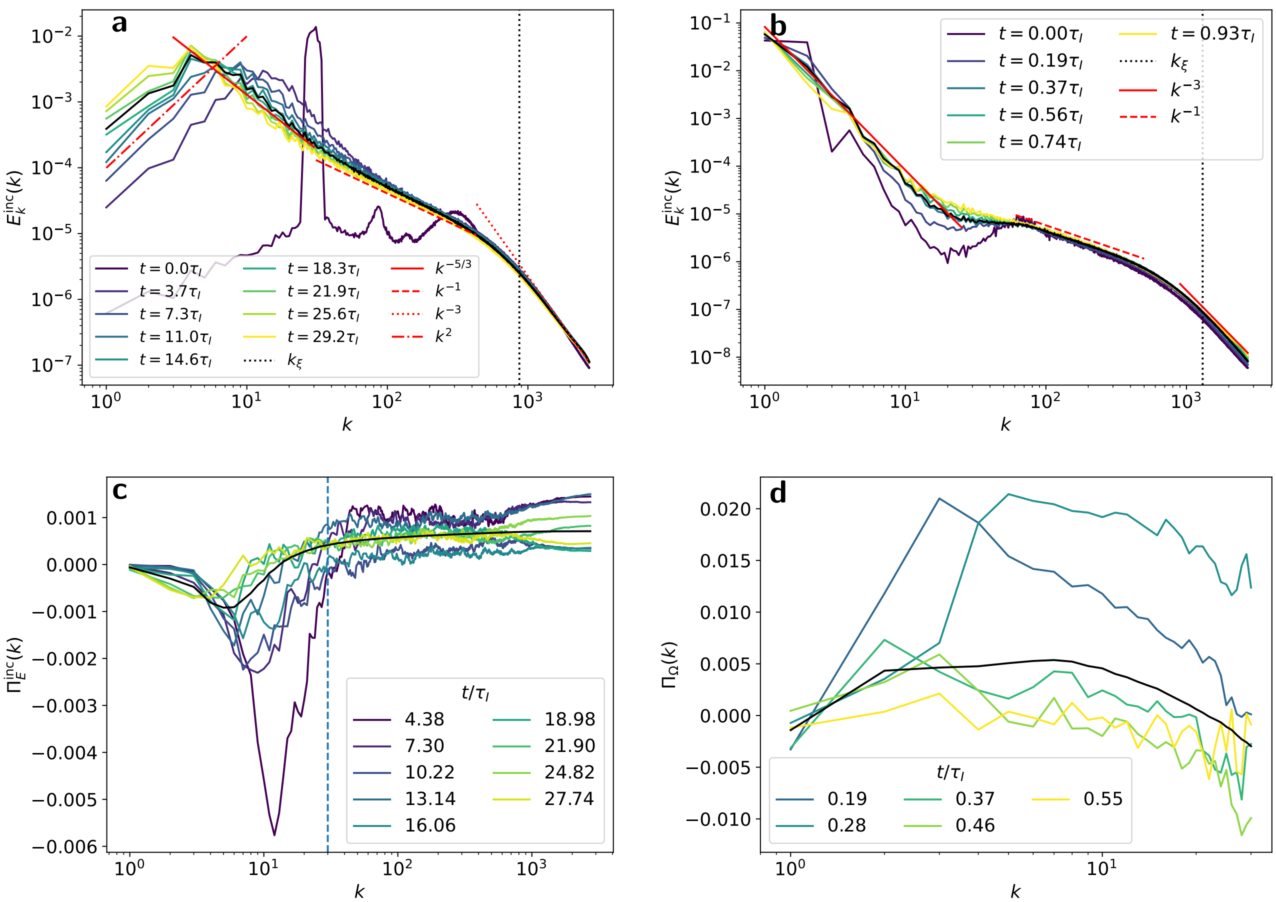

FIG. 2. Evolution of the (a)-(b) incompressible energy spectra, (c) incompressible energy flux and (d) enstrophy flux. The left panels correspond to the inverse energy cascade and the right panels to the direct enstrophy cascade simulations. Black solid lines correspond to temporal averages.

method used in classical and quantum decaying turbulence [1, 4–6]. Figure 1 shows the evolution of the different energy components of the GP-inv and GP-dir-M03 simulations. We made sure that in the whole turbulent regime, the incompressible kinetic energy (the one displaying Kolmogorov-like properties and the relevant one for circulation) is larger than the other components at all times. Time is normalized by the turnover time $\tau_I = v_{\mathrm{rms}}/L_0$ with L_0 the initial integral length scale.

Figure 2 (a) and (b) show the evolution of the energy spectra in the GP-inv and GP-dir-M03 simulations, respectively. In the former case, we excite the flow at a range of wave numbers centered at $k_0 \approx 30$. As it evolves, the peak of the spectra moves to larger scales, a signature of an inverse energy cascade process [2]. Among the different scales and different times, we observe the development of different scaling laws. At scales larger than the peak, there is a k^2 scaling law that is larger than the expected scaling of energy equipartition k^1. The origin of this scaling regime is not completely clear and further studies are left for future work. Between the spectral peak and k_0, there is a range of scales in which the fluid develops Kolmogorov-like scaling properties, satisfying a $-5/3$ scaling law. Scales smaller than k_0 also correspond to scales smaller than the intervortex distance, as in the case of IEC simulations $k_0 \approx k_\ell$, so we observe the development of a k^{-1} energy spectrum given by individual vortex lines. Finally, at scales smaller than the healing length, dispersive effects dominate and we enter a k^{-3} scaling regime [7]. For the DEC, initially, the flow at large scales develops a k^{-4} scaling property and as it evolves it approaches the k^{-3} scaling law predicted by Kraichnan, neglecting logarithmic corrections [8]. At scales smaller than the intervortex distance, the scaling laws of individual vortex lines are again recovered, as in the IEC cascade.

The individual observation of the celebrated $k^{-5/3}$ and k^{-3} scaling laws in the incompressible energy spectra are not enough to establish the presence of an inverse and direct cascade, respectively. These scaling laws should also

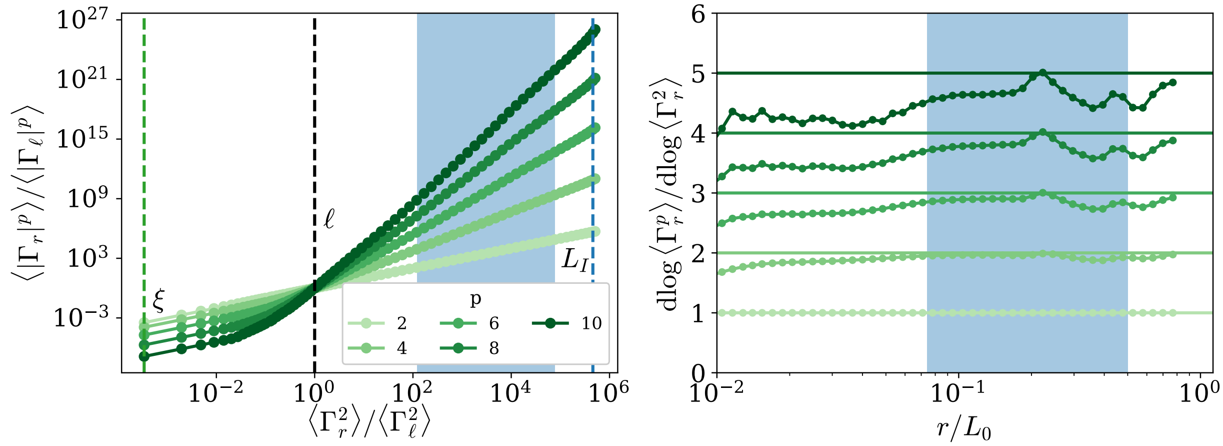

FIG. 3. Circulation moments in numerical simulation of GP-dir-M05 run up to $p = 10$. The blue-shaded area corresponds to the inertial range in which the scaling exponents shown in Fig. 4 of the main text are computed.

be accompanied by constant energy and enstrophy fluxes, as shown in Fig. 2 (c)-(d). We define the incompressible energy and enstrophy fluxes as [2]

$$\Pi_E^{\rm inc}(k) = -\sum_{\tilde{k}=1}^{\tilde{k}=k} \frac{\mathrm{d}E_k^{\rm inc}(\tilde{k})}{\mathrm{d}t} \tag{6}$$

$$\Pi_\Omega(k) = -\sum_{\tilde{k}=1}^{\tilde{k}=k} \tilde{k}^2 \frac{\mathrm{d}E_k^{\rm inc}(\tilde{k})}{\mathrm{d}t}. \tag{7}$$

Indeed, in the IEC simulations for some intermediate times, there is a range of scales where $\Pi_E^{\rm inc} < 0$ and is almost constant. Note that $\Pi_E^{\rm inc}(k_{\rm max}) > 0$ meaning that incompressible energy is transferred to the other components at small scales. For the DEC cascade, we observe the signature of an enstrophy cascade as $\Pi_\Omega > 0$ and almost constant for $k_0 < k < k_\ell$. We show only the enstrophy flux for scales larger than the intervortex distance as it is not properly defined at smaller scales due to the singular nature of quantum vortices. Black solid lines show temporal averages of the different quantities.

High-order moments of circulation in the GP-inv and GP-dir-M03 are shown in the main text of this manuscript. To compare, we include in Fig. 3 the circulation moments of run GP-dir-M05, in which compressible effects can not be neglected. In this case, we observe some deviations from the self-similar prediction for the direct cascade of $\lambda^{\rm DEC} = 2p$, suggesting that the development of quasi-shocks enhances the intermittent behavior of the flow.

CIRCULATION MOMENTS IN NAVIER–STOKES

In both the DEC and IEC regimes of 2D classical turbulence, we study the statistics of circulation and characterize its intermittent behavior. Figure 4 shows the circulation moments $\langle\Gamma_r^p\rangle$ up to $p = 16$ for the IEC and $p = 10$ for the DEC. The insets show the local slopes, defined as the logarithmic derivatives $\mathrm{d}\log\langle\Gamma^p\rangle/\mathrm{d}\log r$. For the IEC, the local slopes display a deviation from the self-similar prediction $\lambda_p^{\rm IEC} = 4p/3$ within the inertial range of scales indicated as the gray shaded area. In the DEC regime, we use the extended-self-similar (ESS) method with respect to $\langle\Gamma_r^2\rangle$ and obtain that the scaling exponents become self-similar following the prediction $\lambda_p^{\rm DEC} = 2p$.

To check for the convergence of these moments, we make sure that the integrands $\Gamma^p P(\Gamma)$ go to zero when $\Gamma \to \pm\infty$. If this condition is not satisfied, it means that there is not enough statistics to study high-order moments. These integrands are shown in Fig. 5. Indeed, we observe that for the studied order moments the probability distribution functions (PDFs) in the IEC and DEC regimes are well resolved for length scales within the inertial range. The bottom panels show the circulation integrands for the Gross–Pitaevskii GP-inv and GP-dir-M03 simulations, again displaying a good convergence.

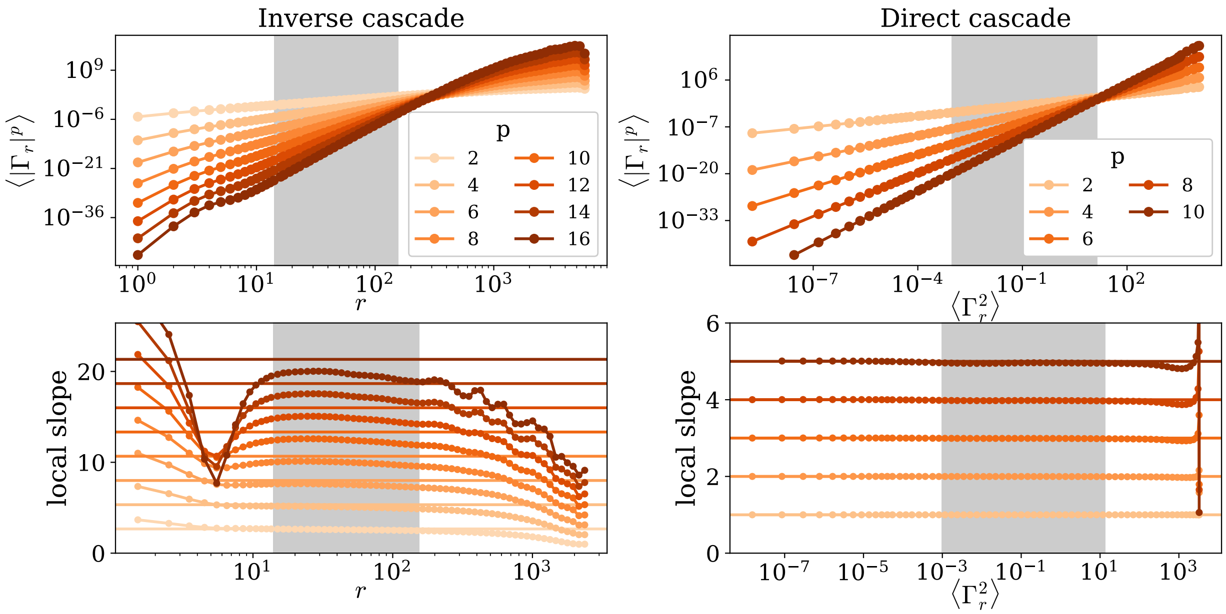

FIG. 4. Circulation moments in numerical simulation of the 2D Navier–Stokes equations for (left panel) the inverse energy cascade up to order $p = 16$ and (right panel) the direct enstrophy cascade up to $p = 10$. For the DEC, we use the extended-self-similar (ESS) hypothesis and plot as a function the moments of $\langle \Gamma_r^2 \rangle$. The bottom panels display the local slopes defined as the logarithmic derivatives of the moments of order p.

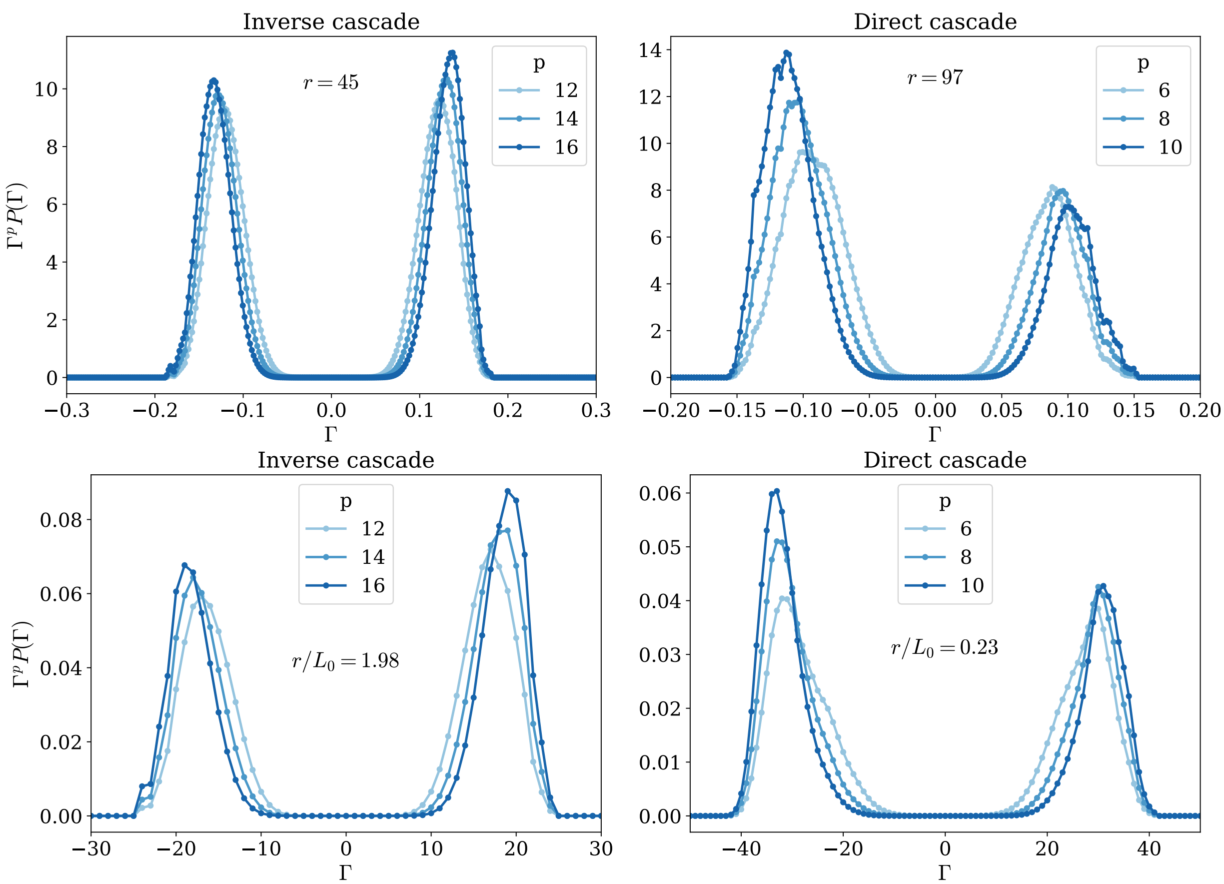

FIG. 5. Circulation integrands for (top panel) 2D classical turbulence and (bottom panel) quantum turbulence in the inverse and direct cascade regimes for a length scale within the inertial range.

MOVIES

We include the time evolution of the 2D GP dynamics in four different numerical simulations. The movies are scatter plots of the positions of positive (red) and negative (blue) individual vortices extracted from the wave function using a circulation-based algorithm. For some frames, this algorithm fails to find some of the vortices. Three movies correspond to one of the individual runs from the ensemble called the GP-dir-M03, GP-dir-M05 and GP-inv in the main manuscript. We provide a fourth movie that shows a longer evolution of the flow in the inverse cascade.

The movies are:

- *gp2d_8192_k1_M03.mp4*: Evolution of the GP-dir-M03 run. Initial condition generated at $k_0 = 1$ with a Mach number $M = 0.3$.
- *gp2d_8192_k1_M05.mp4*: Evolution of the GP-dir-M05 run. Initial condition generated at $k_0 = 1$ with a Mach number $M = 0.5$. Compressible effects become more evident.
- *gp2d_8192_k30.mp4*: Evolution of the GP-inv run. Initial condition generated at $k_0 = 30$.
- *gp2d_8192_k20.mp4*: Extra movie not analyzed in the manuscript. Initial condition generated at $k_0 = 20$.

[1] C. Nore, M. Abid, and M. E. Brachet, Decaying Kolmogorov turbulence in a model of superflow, Physics of Fluids **9**, 2644 (1997).
[2] N. P. Müller, M.-E. Brachet, A. Alexakis, and P. D. Mininni, Abrupt Transition between Three-Dimensional and Two-Dimensional Quantum Turbulence, Physical Review Letters **124**, 134501 (2020).
[3] V. Shukla, M. Brachet, and R. Pandit, Turbulence in the two-dimensional Fourier-truncated Gross–Pitaevskii equation, New Journal of Physics **15**, 113025 (2013).
[4] P. D. Mininni and A. Pouquet, Inverse cascade behavior in freely decaying two-dimensional fluid turbulence, Physical Review E **87**, 033002 (2013).
[5] P. Clark di Leoni, P. D. Mininni, and M. E. Brachet, Dual cascade and dissipation mechanisms in helical quantum turbulence, Physical Review A **95**, 053636 (2017).
[6] C. F. Barenghi, V. S. L'vov, and P.-E. Roche, Experimental, numerical, and analytical velocity spectra in turbulent quantum fluid, Proceedings of the National Academy of Sciences of the United States of America **111**, 4683 (2014).
[7] G. Krstulovic and M. Brachet, Comment on "Superfluid Turbulence from Quantum Kelvin Wave to Classical Kolmogorov Cascades", Physical Review Letters **105**, 129401 (2010).
[8] R. H. Kraichnan, Inertial Ranges in Two-Dimensional Turbulence, Physics of Fluids **10**, 1417 (1967).